Green, red and infrared Er-related emission in implanted GaN:Er and GaN:Er,O samples

T. Monteiro,[a] J. Soares, and M. R. Correia
Departamento de Física, Universidade de Aveiro, 3810-193 Aveiro, Portugal

E. Alves
Instituto Tecnológico e Nuclear, EN10, 2686-953 Sacavém, Portugal

(Received 22 August 2000; accepted for publication 8 March 2001)

Er-related luminescence near 1.54 μm (~805 meV) is observed under below band gap excitation at 4.2 K in GaN:Er and GaN:Er,O implanted samples. The spectrum of the recovered damage samples is a multiline structure. So far, these lines are the sharpest ones reported for GaN. Well-resolved green and red luminescences are observed in implanted samples. The dependence of luminescence on the excitation energy as well as the influence of different nominal fluence and annealing conditions is discussed. Combining the results obtained from photoluminescence and Rutherford backscattering spectrometry, different lattice sites for the optical active Er-related centers are identified. © *2001 American Institute of Physics.* [DOI: 10.1063/1.1369404]

INTRODUCTION

Optically active centers near 1.54 μm (~805 meV) in Er and Er,O implanted GaN epitaxial layers, have been reported in the last five years.[1–13] These are due to the intraionic transition of the Er^{3+} between the two lowest spin- orbit levels $^4I_{13/2} \rightarrow {}^4I_{15/2}$. Besides the well known infrared emission, visible luminescence from higher excited levels was also observed in molecular beam epitaxy (MBE)[8–10] and reactive sputtering[11] grown samples.

The ~1.54 μm photoluminescence (PL) increases with the Er concentration until it reaches saturation.[1] The presence of oxygen promotes an enhancement of the PL intensity[1,8] as well as a reduction of the Er^{3+} PL quenching under below band gap excitation.[8] From PL and photoluminescence excitation different set of PL lines have been assigned to different Er site locations and/or Er–O (or other defects and impurities) related complexes.[2–8,10–13] Lines with full widths at half maximum (FWHM) larger than 1 meV are currently observed.

In this work we study the optical features observed at 4.2 K of implanted GaN:Er and GaN:Er,O samples, under steady-state conditions and under below band gap excitation. As indicated by Rutherford backscattering spectroscopy (RBS) the lattice recovery is better in samples without oxygen. For these samples the PL spectra at 4.2 K shows the highest intensity and the sharpest Er-related emission lines observed in GaN (FWHM of ~0.4 meV for the main line peaked at ~1.538 μm). Well-resolved visible luminescence in the green and red spectral region was identified in implanted samples.

EXPERIMENTAL DETAILS

Samples were cut from high quality (0001) GaN epilayers, with 1.5 μm thickness, grown on sapphire substrates. The intrinsic *n*-type background doping was of the order of 10^{16} cm^{-3}. The five samples indicated in Table I were analyzed. All the Er doses were implanted at 160 keV. The measured implantation range (R_p) was about 40 nm in agreement with TRIM98 calculations. The energy of the O ions was 25 keV in order to obtain the overlap of the O and Er profiles. After the implantation all samples were annealed at 650 °C under flowing nitrogen, using another GaN sample as a proximity cap. Before the second annealing step, sample C was annealed at 1000 °C for 20 min under the same conditions. All the samples were then submitted to a further annealing under nitrogen overpressure of 1 GPa at 1200 °C for 20 min, except sample D that was annealed a second time in these conditions.

The infrared spectral region PL measurements have been performed with a Brucker 66V Fourier-transform spectrometer. The signal was detected with a North-Coast EO-817 liquid nitrogen cooled germanium detector. The 476, 488, 496.4, 501, and 525 nm lines of an Ar laser were used for below band gap excitation. The samples, immersed in liquid He, were placed on a cold finger of a continuous-flow cryostat in vacuum. For the visible spectral region above and below band gap excitation either a Xe lamp, coupled to a monochromator, and the 514.5 nm line of an Ar laser were used. Time resolved spectra were carried out with a pulsed Xe lamp as an excitation source and a boxcar system for

TABLE I. Sample characteristics.

Sample	Implantation dose (ion cm^{-2}) Er	Implantation dose (ion cm^{-2}) O	Implantation temperature (°C)
A	5×10^{14}	···	550
B	5×10^{15}	···	550
C	5×10^{15}	···	RT
D	5×10^{15}	5×10^{15}	RT
E	5×10^{14}	5×10^{14}	RT

[a]Electronic mail: tita@fis.ua.pt

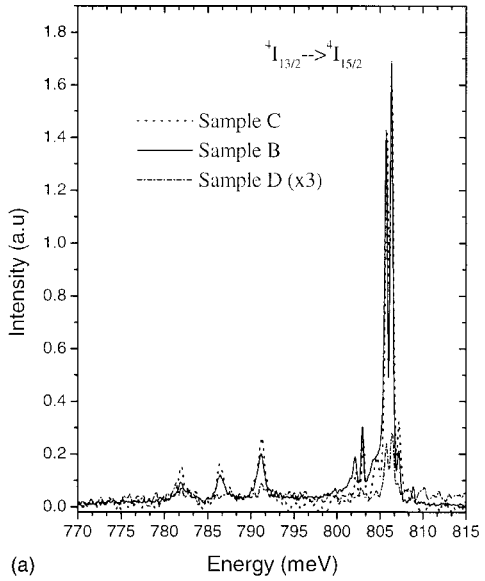

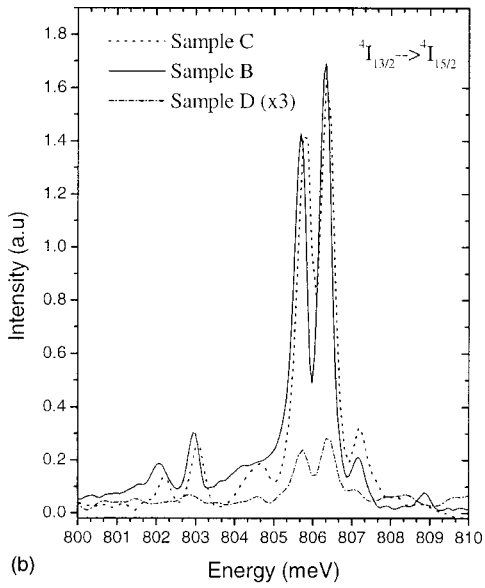

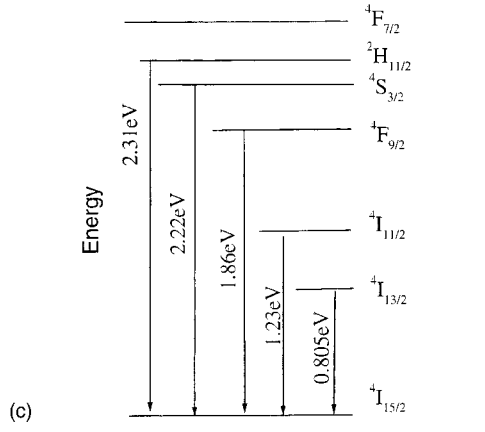

FIG. 1. (a) PL spectra of samples B, C, and D obtained under below band gap excitation, $\lambda_{exc}=496.4$ nm at 4.2 K. Sample B: high temperature Er implanted sample with 5×10^{15} cm^{-2}; sample C: room temperature Er implanted sample with 5×10^{15} cm^{-2}; and sample D: room temperature co-implanted sample with the same dose of samples B and C. (b) Enlarged high energy spectrum of Fig. 1(a) showing the split of PL lines for high and RT temperature implanted samples (samples B and C) as well as for the room temperature co-implanted sample (sample D). (c) Simplified energy diagram of Er^{3+} in GaN. The energy of PL emission lines are also shown.

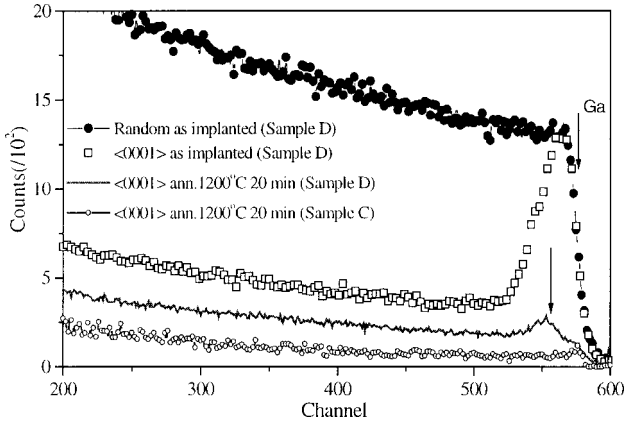

FIG. 2. Random and ⟨0001⟩ aligned RBS spectra of samples C and D before and after annealing. The arrow marks the presence of residual damage in the implanted region of sample D after the annealing.

detection (time range from hundreds of microns to seconds). In both cases the luminescence was dispersed by a Spex 1704 monochromator and detected by a photomultiplier.

RBS/channelling studies were performed with a 1 mm diameter collimated beam of $^4He^+$ with 2.0 MeV. The backscattered particles were detected at 140° and close to 180°, with respect to the beam direction, using silicon surface barrier detectors located in the standard IBM geometry and with resolutions of 13 and 16 keV, respectively.

RESULTS AND DISCUSSION

In Fig. 1(a) the 4.2 K Er-related infrared emission excited by the 496.4 nm line of an Ar laser for samples B, C, and D is shown. In Fig. 1(b) an enlarged spectrum of the high-energy side is presented. Despite the differences in intensity of the lines, the multiline structure is identical for high and room temperature implanted samples with the same nominal Er fluence (samples B and C), as well as for the oxygen co-implanted sample with the same dose (sample D). This indicates that the same Er-related centers are present in Er and Er,O implanted samples. We also found, for sample B, a slight shift to lower energies on the main lines that could be attributed to residual strain in the sample. From Figs. 1(a) and 1(b) it is also evident that the PL intensity of the Er implanted samples is nearly independent of the implantation temperature (samples B and C). We observed an enhancement of PL intensity for samples without oxygen co-implantation, in contrast with previous ones.[1] The quenching of PL emission can be related with the presence of oxygen related complexes. Residual defects are evident on the RBS aligned spectrum of Fig. 2, for co-implanted sample D. Before the annealing the aligned spectra of both samples are identical. The amount of damage created by the implantation is enough to produce an overlap of the random and aligned spectra in the whole implanted region (55 nm), indicating the complete amorphization of this region. The high temperature annealing procedure used in our work result in the complete recrystallization of the damage layer, situation impossible to achieve with lower annealing temperatures.[14] However, in the oxygen co-implanted sample, the remaining defects are

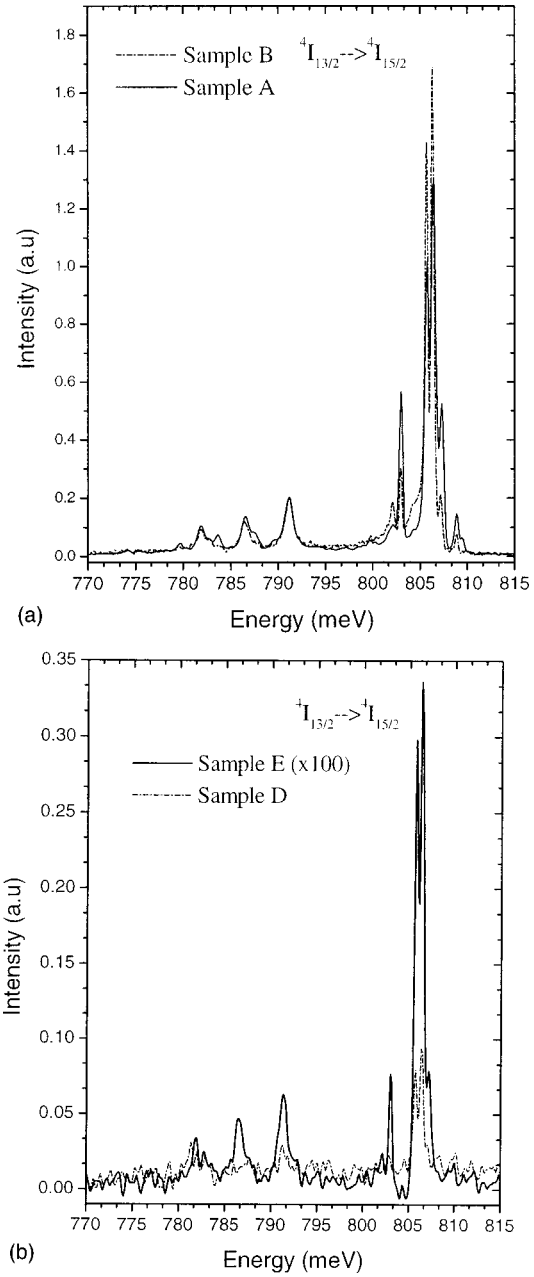

FIG. 3. (a) PL spectra of samples A and B obtained under below band gap excitation, $\lambda_{exc}=496.4$ nm at 4.2 K. Samples A and B: high temperature Er implanted with 5×10^{14} cm^{-2} and 5×10^{15} cm^{-2}, respectively. (b) PL spectra of samples D and E obtained under below band gap excitation, $\lambda_{exc}=496.4$ nm at 4.2 K. Samples D and E: room temperature co-implanted samples with doses of 5×10^{15} cm^{-2}, and 5×10^{14} cm^{-2}, respectively. Sample D was submitted to a two stage annealing process.

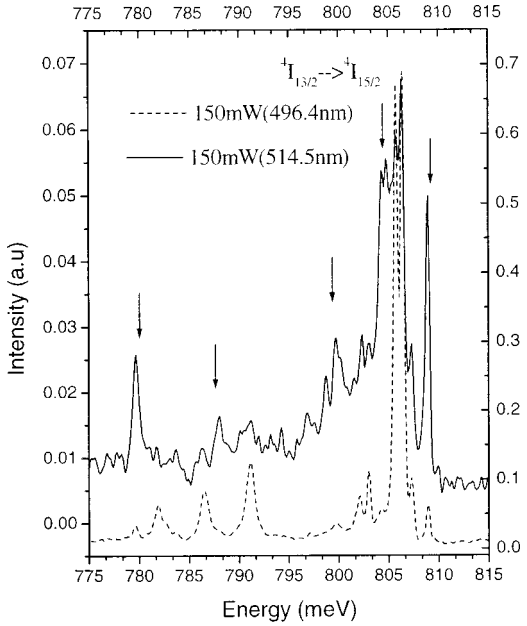

FIG. 4. Energy excitation PL dependence at 4.2 K for sample A (high temperature implanted GaN:Er sample with 5×10^{14} cm^{-2}).

responsible for the increase in the dechanneling rate observed in the aligned spectrum (as indicated by the arrow in Fig. 2). The high mobility of oxygen in GaN above 1000 °C could be the reason for the presence of these stable defects and explain why they were not formed in cases of lower temperature annealing.

In all the cases the increase of the implanted fluence is followed by an increase on PL intensity, as shown in Fig. 3(a) for samples A and B (high temperature Er implanted samples). Figure 3(b) shows similar results for room temperature co-implanted samples (D and E). From the spectra of Fig. 3 it is important to note that while the main lines at 806.3 and 805.7 meV, with FWHM of ~0.4 meV, decrease in intensity the lines at 808.8, 807.3, and 803 meV are enhanced in sample A (lower Er fluence). This indicates that in sample A, these related energy states are preferentially populated than in sample B.

The dependence of luminescence on the excitation energy is presented in Fig. 4. Apart from a change in intensity, it is clear that different emission lines are favored when the excitation energy changes, as indicated by arrows in Fig. 4. From these data we can assume that different Er-related optical centers are involved. The presence of Er occupying different lattice locations or forming complexes with O or other impurities are currently assigned as responsible for the different optical centers.[2–6]

The existence of Er in different lattice sites of the GaN structure was confirmed by the detailed channeling angular scans along the ⟨0001⟩ and ⟨1011⟩ axes. The results in Fig. 5 show the angular scans through these axes for sample B, after annealing. To evaluate the Er fractions in different lattice sites the data were fitted (continuous curves) with the simulations from a Monte Carlo code.[15] The results show the complete overlap of the Er and Ga curves along the ⟨0001⟩ direction [Fig. 5(a)] which is an indication that Er is placed along the mixed Ga–N rows of atoms, as indicated in the projection. The high value of the minimum yield indicates the presence of some residual damage in the sample that could be the cause of the strain responsible for the shift in the PL lines mentioned before. The best fit obtained with the simulation reveals the presence of 47% of Er substitutional along this direction and 53% in random places. The scan across the tilt ⟨1011⟩ axis [Fig. 5(b)], where we have pure Ga and N rows (see the projection), allows us to establish if Er is in Ga or N places or even displaced along the ⟨0001⟩ axis. In this tilt direction the best fit of the experimental results,

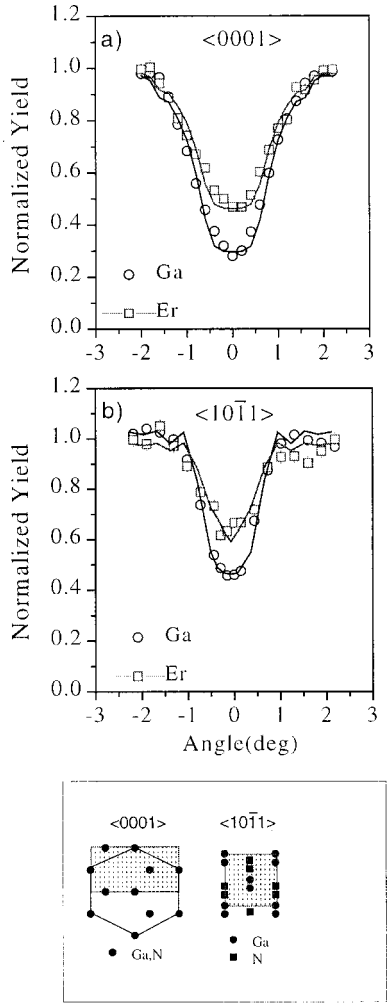

FIG. 5. Angular scans along the ⟨0001⟩ and ⟨101⟩ axes for sample B after annealing. The projections on the plane perpendicular to each direction. The continuous lines are the results of the Monte-Carlo simulations.

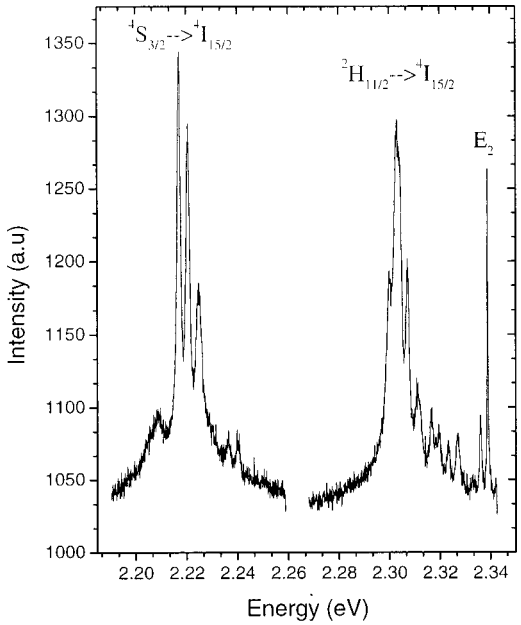

FIG. 6. High excitation density luminescence spectra of sample A obtained under below band gap excitation at RT. The spectra were obtained in a Jobin Yvon–Spex T64000 using the 514.5 nm line of an Ar ion laser as excitation source.

represented by the continuous curve, was obtained assuming that 32% of the Er is occupying Ga lattice sites, a fraction of 13% displaced along the ⟨0001⟩ axis and the remaining 55% are randomly distributed. The displaced fraction accounts for the narrowing observed in the bottom of the Er angular curve. Notice that the random fraction could correspond to different amounts of Er, placed in low symmetry sites, difficult or impossible to find by the channeling technique. Nevertheless, the coherence of the results in both directions led us to conclude that, after the annealing, Er is incorporated at least in two well defined sites of the GaN structure.

It is known from recent reports[8–11] that luminescence from higher excited states in the visible spectral region was observed in MBE and reactive sputtering grown samples. Namely green lines from $^2H_{11/2}\rightarrow{}^4I_{15/2}$ and $^4S_{3/2}\rightarrow{}^4I_{15/2}$ at 2.31 eV (537 nm) and 2.22 eV (558 nm) have been found by several authors[8–11] as well as minor peaks assigned to $^2H_{9/2}\rightarrow{}^4I_{15/2}$ at 3.0 eV (413 nm), $^4F_{5/2}\rightarrow{}^4I_{15/2}$ at 2.69 eV (461 nm), $^4F_{9/2}\rightarrow{}^4I_{15/2}$ at 1.86 eV (665 nm), and $^4F_{5/2}\rightarrow{}^4I_{13/2}$ at 1.76 eV (706 nm).

In Fig. 6 the Raman spectra of sample A performed with a 514.5 nm line of an Ar laser at room temperature is shown. Besides the E_2-high phonon mode from GaN lattice,[16] well resolved luminescence in the green region near 2.31 eV (537 nm) and 2.22 eV (558 nm) is observed in implanted metal-organic chemical vapor deposition (MOCVD) grown samples. Green emission is confirmed by the anti-Stokes Raman spectra (not shown). Main lines separated by 2–3 meV apart with FWHM of ~2 meV can be identified at 2.310, 2.307, 2.304, 2.302, and 2.299 eV for the $^2H_{11/2}\rightarrow{}^4I_{15/2}$ transition and 2.226, 2.224, 2.220, and 2.217 eV, for the $^4S_{3/2}\rightarrow{}^4I_{15/2}$ transition. Furthermore minor peaks on the high energy side of each group of lines with a nearly constant 3 meV separation are also observed. The same spectrum was observed for samples B and C, while for the co-implanted samples the yellow luminescence dominates the spectra.

The intra $4f$ transitions are parity forbidden, however, they can be observed due to a mixing with the $4f5d$ state. As long lived states are expected,[17] time resolved PL (TRPL) measurements were performed. In Fig. 7, the TRPL spectra of sample A between 0.1 and 10 ms after the pulse excitation is shown. As green lines have an average lifetime of 5.5 μs at RT,[10] they cannot be observed within our set-up resolution. However the red lines from the $^4F_{9/2}\rightarrow{}^4I_{15/2}$ transition are identified near 1.86 eV (665 nm). The splitted red lines occur at 1.92 eV (645.8 nm), 1.88 eV (659.4 nm), 1.85 eV (670 nm), 1.83 eV (677.5 nm), and 1.82 eV (681 nm). The FWHM of the lines varies between 5 and 10 meV. The lines are best resolved at RT than 11 K. All the set of studied samples shows the same red lines as can be observed from Figs. 7(a) and 7(b). From the same figure it is clear that the slow emission on the yellow spectral region is sample dependent. The studied samples reveal that a complete lattice recovery can be achieved after annealing. As shown in Fig. 6 the E_2-high phonon mode of the GaN lattice is clearly identified. On the other hand, under band to band excitation,

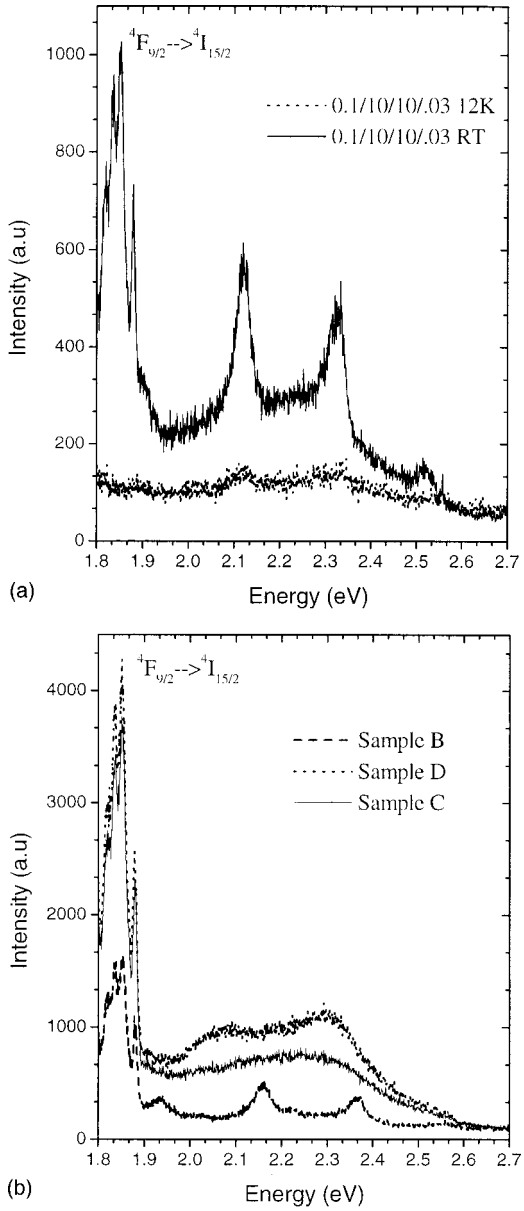

FIG. 7. (a) Time resolved spectra performed under total excitation between 0.1 and 10 ms after the pulse excitation at 11 K and RT for sample A. (b) Time resolved spectra performed under total excitation between 0.1 and 10 ms after the pulse excitation at RT for samples B, C, and D.

similar PL spectra of unimplanted GaN samples[18,19] can be observed in the visible region as shown in Fig. 8.

CONCLUSIONS

In RT and high temperature implanted GaN:Er and GaN:Er,O samples the sharpest zero phonon lines (FWHM ~0.4 meV), observed in infrared Er-related PL centers under below band gap excitation in GaN samples, were detected. The multiline spectra and its dependence on the fluence and excitation energy clearly indicate that different Er-related optical centers located in different lattice site symmetries are responsible for the emission. Well-resolved green, red, and infrared luminescence from Er related centers were observed both in Er and Er,O implanted MOCVD grown GaN samples. From the time resolved spectra, lifetimes of the

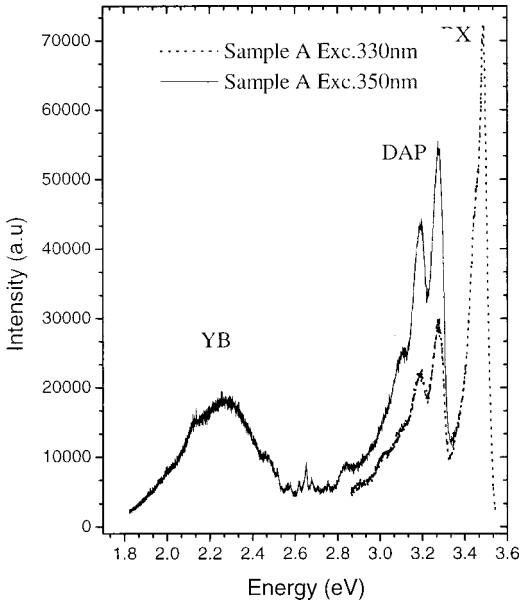

FIG. 8. Uncorrected PL spectra obtained for sample A by above band gap excitation using a Xe lamp coupled to a monochromator at 11 K.

order of microseconds are observed for the red lines while lifetimes below hundreds of microseconds for the green lines are found, in agreement with previous reports.

The results clearly show that the damage recovery in GaN is possible by annealing at high temperature under high nitrogen pressure, as indicated by the RBS measurements as well as by the optical experiments. The annealing at 1200 °C allows the complete epitaxial regrowth of the amorphous layer and the incorporation of some Er into well defined sites of the GaN lattice. After the annealing the PL signal is more intense in samples without oxygen that may be due to a better lattice recovery on these samples. The increase in the GaN yellow band on the co-implanted samples is also an indication of a high number of defects in the GaN lattice, which may explain the decrease in Er related green emission.

ACKNOWLEDGMENT

The authors wish to thank E. Pereira for fruitful comments.

[1] J. T. Torvik, C. H. Qiu, R. J. Feuerstein, J. I. Pankove, and F. Namavar, J. Appl. Phys. **81**, 6343 (1997).
[2] J. T. Torvik, R. J. Feuerstein, C. H. Qiu, J. I. Pankove, and F. Namavar, J. Appl. Phys. **82**, 1824 (1997).
[3] S. Kim, S. J. Rhee, D. A. Turnbull, X. Li, J. J. Coleman, S. G. Bishop, and P. B. Klein, Appl. Phys. Lett. **71**, 2662 (1997).
[4] S. Kim, S. J. Rhee, D. A. Turnbull, X. Li, J. J. Coleman, and S. G. Bishop, Mater. Res. Soc. Symp. Proc. **468**, 131 (1997).
[5] S. Kim, X. Li, J. J. Coleman, R. Zhang, D. M. Hansen, T. F. Kuech, and S. G. Bishop, MRS Internet J. Nitride Semicond. Res. **4S1**, G11.4 (1999).
[6] M. Thaik, U. Hömmerich, R. N. Schwartz, R. G. Wilson, and J. M. Zavada, Appl. Phys. Lett. **71**, 2641 (1997).
[7] E. Alves *et al.*, Mater. Sci. Eng., B (to be published).
[8] U. Hömmerich, J. T. Seo, M. Thaik, J. D. MacKenzie, C. R. Abernathy, S. J. Pearton, R. G. Wilson, J. M. Zavada, MRS Internet J. Nitride Semicond. Res. **4S1**, G11.6 (1999).
[9] M. Garther, R. Birkhahn, A. J. Steckl, and J. Scofield, MRS Internet J. Nitride Semicond. Res. **4S1**, G11.3 (1999).
[10] U. Hömmerich, J. T. Seo, J. D. MacKenzie, C. R. Abernathy, R. Birkhahn,

A. J. Steckl, and J. M. Zavada, MRS Internet J. Nitride Semicond. Res. **5S1**, W11.5 (2000).
[11] H. Chen, K. Gurumugan, M. E. Kordesh, W. M. Jadwisenczak, and H. J. Lozykowski, MRS Internet J. Nitride Semicond. Res. **5S1**, W3.6 (2000).
[12] S. Kim, S. J. Rhee, X. Li, J. J. Coleman, and S. G. Bishop, Appl. Phys. Lett. **76**, 2403 (2000).
[13] S. Kim, S. J. Rhee, J. O. White, A. M. Mitofsky, X. Li, G. C. Papen, J. J. Coleman, and S. G. Bishop, Mater. Sci. Eng. B (to be published).
[14] E. Alves, M. F. da Silva, J. C. Soares, R. Vianden, J. Bartels, and A. Kozanecky, Nucl. Instrum. Methods Phys. Res. B **147**, 383 (1999).
[15] E. Alves, M. F. da Silva, J. C. Soares, R. Vianden, C. R. Abernathy, and S. J. Pearton, MRS Internet J. Nitride Semicond. Res. **4S1**, G11.2 (1999).
[16] T. Azuhata, T. Sota, K. Suzuki, and S. Nakamura, J. Phys. C **7**, L129 (1995).
[17] G. Blasse and B. C. Grabmaier, *Luminescence Materials* (Springer, Berlin, 1994).
[18] B. Gil, *Group III Nitride Semiconductors Compounds Physics and Applications* (Oxford, New York, 1998).
[19] R. Seitz, C. Gaspar, T. Monteiro, E. Pereira, M. Leroux, B. Beaumont, and P. Gibart, MRS Internet J. Nitride Semicond. Res. **2**, 36 (1997).